

Combined Galileo/GPS Architecture for Enhanced Sensitivity Reception

Andreas Schmid, André Neubauer, Henning Ehm, Robert Weigel, Norbert Lemke, Günter Heinrichs, Jon Winkel, Jose Angel Ávila-Rodríguez, Roland Kaniuth, Thomas Pany, Bernd Eissfeller, Günter Rohmer, Bernhard Niemann, and Matthias Overbeck

Abstract Several new requirements and challenges are introduced with the transition of traditional navigation applications towards location based services. This paper introduces the HIGAPS receiver concept. Aim of the HIGAPS project is to develop the concept for a combined Galileo/GPS receiver that is specially tailored for location based services, E-911, and other consumer market applications. After a brief overview of the receiver, the partitioning into analog hardware, digital hardware, and software is outlined. The architecture of the combined Galileo/GPS RF front-end is presented in low-IF topology. The digital baseband presents a highly parallel correlation architecture for combined Galileo/GPS reception, allowing moderate times to fix for extended dwell times. Parallel digital signal processing combined with aiding data allows single shot measurements particularly designed for location based services. Differential correlation, where the current coherently integrated predetection sample is multiplied with the conjugated complex of the previous predetection sample further improves the reception sensitivity.

Keywords Galileo, GPS, Architecture, Enhanced Sensitivity

1. Introduction

Most GNSS market surveys anticipate an exponentially increasing market for location based services that may soon become the major consumer market GNSS application. Location based services, including the U.S. E-911 mandate, however, exhibit distinctly different requirements that cannot be met by traditional navigation receivers.

The undoubtedly most important prerequisite for a GNSS receiver in location based services and consumer market applications is very low cost. The HIGAPS concept is therefore based upon newest high integration CMOS technology and establishes a concept with fewest external components. Advanced digital signal processing that

is especially designed for low implementation complexity further reduces costs and power consumption.

Low energy consumption is particularly important, since most host systems for location based services are mobile handsets, such as mobile phones or personal digital assistants. The receiver concept therefore allows operation in two distinct modes - stand-alone reception mode and location based services mode. For stand-alone reception, the receiver performs acquisition, tracks the signals and decodes the data overlay. Location based services mode is aided by assistance data as defined in the A-GPS protocols by 3GPP. The receiver only completes a single shot measurement with an extended acquisition to accurately synchronize to the Galileo and GPS signals. Doppler shift estimation and the data overlay are delivered by the assistance network. The short operation period not only results in very low energy consumption, it also enables quick response times.

The third extraordinarily important requirement is high availability of the positioning service. Typical reception sites for location based services include deep urban, moderate indoor, urban canyon, and inside vehicles without external antenna. This frequently introduces an additional attenuation of 25 dB or more on top of free space loss and multipath fading. Assistance data aiding is one means to support the required enhanced reception sensitivity. The architecture of the combined Galileo and GPS receiver also provides an integrated low noise RF front-end and advanced digital signal processing for enhanced sensitivity acquisition. The receiver concept considers an optimal gain combination of coherent, differential, and noncoherent correlation.

2. Receiver Overview

A combined antenna is used for GPS and Galileo. In the RF front-end, the signal is down-converted to an intermediate frequency, where the signal is sampled (i.e. A/D converted). Filtering to reject out-of-band interferences and to block mirror signals is also applied in the front-end. Amplification and down-conversion to intermediate frequency have to be accomplished without changing the signal shape significantly. The conditioned signal from the front-end is feed to the A/D converter, where sampling and quantization takes place.

As part of the digital subsystem the code-phase tracking using a delay-lock-loop (DLL) is implemented additionally to the single shot measurement architecture. Supplementary measures for the BOC signals are necessary due to the multiple correlation peaks. Carrier phase tracking is done using a phase-locked loop (PLL). Coherent corre-

Received month 10, 2004.

Dipl.-Ing. Andreas Schmid, Dr.-Ing. André Neubauer, Development Center Düsseldorf, Infineon Technologies AG, P. O. Box 340129, 40440 Düsseldorf, Germany.

Dipl.-Phys. Henning Ehm, Prof. Dr.-Ing. Dr.-Ing. Robert Weigel, Institute of Electronics Engineering, University Erlangen-Nuremberg, Cauerstrae 9, 91058 Erlangen, Germany.

Dipl.-Ing. Norbert Lemke, Dr.-Ing. Günter Heinrichs, Dr.-Ing. Jon Winkel, IfEN GmbH, Alte Gruber Straße 6, 85586 Poing, Germany.

Dipl.-Ing. Jose Angel Ávila-Rodríguez, Dipl.-Ing. Roland Kaniuth, Dr. Thomas Pany, Prof. Dr.-Ing. Bernd Eissfeller, Institute of Geodesy and Navigation, University FAF Munich, 85577 Neubiberg, Germany.

Dr.-Ing. Günter Rohmer, Dipl.-Ing. Bernhard Niemann, Dipl.-Ing. Matthias Overbeck, Fraunhofer Institute of Integrated Circuits, Am Wolfsmantel 33, 91058 Erlangen, Germany.

Table 1. Proposed partitioning of functionalities between analog hardware, digital hardware, and software.

| Analog Hardware | Digital Hardware | Software |
|--|--------------------------------------|--|
| Downconversion to Intermediate Frequency | Downconversion to Baseband | Assistance Data Processing |
| Local Oscillator | Digital Clock Generation | Visible Satellite Estimation |
| Suppression of the Mirror Frequency | Doppler Shift Compensation | Frequency Deviation Estimation |
| Analog to Digital Conversion | Despreading | Code Phase Estimation |
| | Coherent Integration | Data Bit Estimation |
| | Noncoherent/Differential Integration | Selection of Integration Times |
| | Storage of the Correlation Values | Data Decoding |
| | | Synchronization Lock Detection |
| | | Calculation of the Navigation Solution |

lation combined with differential or noncoherent correlation will be carried out for the pilot channel and the data channel. A hybrid navigation solution is intended to make use of assistance data from the cellular network. The proposed partitioning of receiver functionalities between analog hardware, digital hardware, and software is presented in Table 1.

3. RF Front-End

For the combined Galileo/GPS receiver front-end a low-IF architecture is proposed, shown in Fig. 1. This architecture utilizes the benefits of a competitive, low power and high integration CMOS process. It requires a minimum of off-chip components. The front-end bandwidth is approximately 4 MHz. This comprises the two main lobes of the Galileo BOC(1,1) signal as well as the main lobe of the GPS C/A code with its two side lobes. Compared to a zero-IF architecture, the low-IF architecture is insensitive to DC-offsets and flicker noise. Both problems can be avoided by AC-coupling between consecutive stages in the front-end. In zero-IF GPS receivers AC-coupling is a major problem, since most of the GPS C/A code signal energy is at DC. The main drawbacks of the low-IF architecture are its limited image rejection and the stringent I/Q-mismatch requirements. Both issues are relaxed in a combined low-IF Galileo/GPS receiver, when the IF is below 8 MHz. For this choice the image lies in the Galileo/GPS-L1 band and mainly consists of thermal noise. In this case, an image reject ratio

$$IIR = \frac{\left(\frac{\Delta A}{2A}\right)^2 + \tan^2\left(\frac{\Delta\phi}{2}\right)}{1 + \left(\frac{\Delta A}{2A}\right)^2 \tan^2\left(\frac{\Delta\phi}{2}\right)} = 20 \text{ dB} \quad (1)$$

is enough to reduce the SNR degradation due to the limited image rejection below 0.1 dB. In (1) ΔA denotes the amplitude difference and $\Delta\phi$ the phase difference between the I- and Q-path. This IIR can be achieved with moderate limits for the amplitude and phase error in the I/Q-path. For an amplitude error of $(\Delta A + A)/A = 1 \text{ dB}$ and a phase error of $\Delta\phi = 4$ the IIR, due to I/Q-mismatch, is approximately 24 dB.

Fig. 1 shows the detailed front-end architecture of the signal path. The signal received from the antenna is directly fed into the input of the front-end. The signal is amplified by the first low noise amplifier (LNA) and fed to

the off-chip bandpass filter (BPF). From there the signal is fed back into the chip, where it is further amplified by a second LNA. The LNA is followed by a quadrature mixer which downconverts the signal to a low IF of 3.5 MHz. The signal is amplified after the mixer and complex filtered by a polyphase filter

$$H_{\text{Polyphase}}(f) = H_{\text{LP}}(f - f_0), \quad (2)$$

which can be thought of as a frequency shifted lowpass filter [2]. The polyphase filter attenuates the image and rejects out of band noise. The shift frequency f_0 equals the IF in this application. From there the signal is amplified by means of a power controlled amplifier chain (PGC) to a detectable level for analog to digital conversion. The signal is sampled with 3 bits, which is enough to limit the quantization degradation of the SNR to less than 0.75 dB [4]. Since the signal after the polyphase filter is at IF, it is possible to use only the I-path output of the polyphase filter and to neglect the Q-path. The disregard of the Q-path after the polyphase filter slightly reduces the power consumption and the die area of the receiver front-end. Whether this is a good option based on the SNR correlation peak is still under investigation.

Fig. 2 shows the downconversion from the L1 carrier frequency (RF) to baseband. The analysis of the downconversion process and the filtering is preferable done with the help of complex signals [2]. The real bandpass signals in the I- and Q-path are denoted as $x(t)$ and $y(t)$, respectively. Together they can be treated as one complex signal

$$z(t) = x(t) + j y(t). \quad (3)$$

The spectrum of the complex signal $z(t)$ is single sided, if $x(t)$ and $y(t)$ are related through the Hilbert transform \mathcal{H} .

Fig. 2.a shows the spectrum of the signal $S(f)$, the image $I(f)$ and the LO, $e^{-j\omega t}$, before the first mixing process. The spectrum of the LO-signal is single sided, since

$$\mathcal{H}\{\cos(2\pi f_{\text{LO}}t)\} = \sin(2\pi f_{\text{LO}}t). \quad (4)$$

The spectrum of $S(f)$ and $I(f)$ are double sided, since these two are real valued.

Fig. 2.b shows the spectrum after the first mixing process

$$S'(f) + I'(f) = (S(f) + I(f)) \otimes e^{-j2\pi f_{\text{LO}}t}, \quad (5)$$

the convolution of $S(f)$ and $I(f)$ with the LO-signal. The complete spectrum is shifted by f_0 towards negative frequencies. Now the positive part of $S(f)$ is at positive IF,

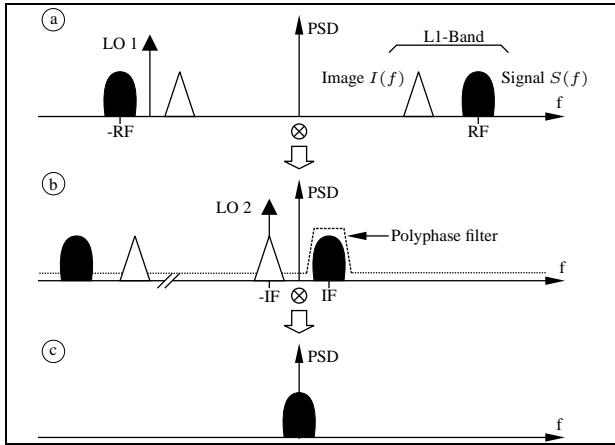


Fig. 2. The downconversion process. (a): The signal and image at positive frequencies are downconverted by the LO 1 signal to the intermediate frequency. (b): The image is cancelled by means of a polyphase filter. In the next step the signal is further downconverted to baseband by means of the LO 2 signal. (c): The signal at baseband.

whereas the positive part of $I(f)$ is at negative IF. The negative parts of $S(f)$ and $I(f)$ are both shifted to higher negative frequencies. With the aid of the polyphase filter, the image at negative IF is filtered out

$$S''(f) + I''(f) = [S'(f) + I'(f)] \cdot H_{\text{Polyphase}}(f). \quad (6)$$

After the image is removed the signal is further downconverted to baseband in a second complex mixing process.

4. Digital Baseband

Parallelized hardware allows the combined Galileo/GPS receiver concept to support substantially long dwell times for enhanced reception sensitivity together with moderate time-to-fix. This parallel signal processing combined with assistance data aiding enables single shot measurements. Fig. 3 visualizes the concept for the parallelized digital baseband processing. The bandpass signal at the output of the common Galileo/GPS RF front-end may be represented by the complex-valued equivalent low-pass signal $r_{lp}(t)$ and the nominal intermediate frequency f_{IF}

$$r_{bp}(t) = \Re \{ r_{lp}(t) \cdot e^{j \cdot 2\pi f_{IF} \cdot t} \}. \quad (7)$$

After the digital downconversion, the result is the low-pass equivalent signal

$$r_{lp}(t) = \sqrt{2C} \cdot d(t) \cdot c(t) \cdot e^{j \cdot \phi(t)} + n(t), \quad (8)$$

where C represents the carrier power, $d(t)$ the data signal, $c(t)$ the received spreading code, $\phi(t)$ the time-variant received signal phase, and $n(t) = n_I(t) + j \cdot n_Q(t)$ the complex-valued zero-mean additive white Gaussian noise

with

$$\begin{aligned} \sigma_n^2 &= E \{ |n - E\{n\}|^2 \} = 2 \cdot E \{ n_I^2 \} = 2 \cdot E \{ n_Q^2 \} \\ &= 2N_0 \cdot B \cdot F \\ &= 2 \cdot 1.38 \cdot 10^{-23} \text{ J/}^\circ\text{K} \cdot 290^\circ\text{K} \cdot B \cdot F, \end{aligned} \quad (9)$$

where F is the receiver noise figure and $B = 1/T_s$ the passband bandwidth of an ideal anti-aliasing filter. T_s is the sample period.

The sampled signal after downconversion to baseband

$$r_\nu = \sqrt{2C} \cdot d_\nu \cdot c_\nu \cdot e^{j \cdot \phi_\nu} + n_\nu \quad (10)$$

is then despread with the local PRN reference code $c_{r,\nu}$ and coherently integrated

$$\begin{aligned} s_\mu &= \sum_{\nu=1}^L r_\nu \cdot c_{r,\nu+\tau \bmod N}^* \\ &= \sqrt{2C} \cdot \sum_{\nu=1}^L d_\nu \cdot c_\nu \cdot c_{r,\nu+\tau \bmod N}^* \cdot e^{j \cdot \phi_\nu} \\ &\quad + \sum_{\nu=1}^L n_\nu \cdot c_{r,\nu+\tau \bmod N}^* \end{aligned} \quad (11)$$

The coherent integration number $L = T_c/T_s$ is the ratio of coherent integration time T_c to sample period T_s and N denotes the sequence period of the PRN code with respect to the sampling rate.

For sufficiently small frequency deviations $\Delta \bar{f}_\mu$, the phase terms $e^{j \cdot \phi_\nu}$ in (11) can be approximated with help of the average frequency deviation $\Delta \bar{f}_\mu$ during one coherent integration interval $[(\mu - 1) \cdot T_c, \mu \cdot T_c]$ and the phase mismatch φ_μ at the beginning of the coherent integration interval. The predetection samples after downconversion, despreading, and coherent integration then result to [7]

$$\begin{aligned} s_\mu &= \sqrt{2C} \cdot d_\mu \cdot R_{rc}(\tau) \cdot \text{si}(\pi \Delta \bar{f}_\mu \cdot T_c) \\ &\quad \cdot e^{j \cdot (\pi \Delta \bar{f}_\mu \cdot T_c + \varphi_\mu)} + w_\mu, \end{aligned} \quad (12)$$

where

$$R_{rc}(\tau) = \sum_{\nu=1}^L c_\nu \cdot c_{r,\nu+\tau \bmod N}^* \quad (13)$$

is the circular cross-correlation function between received code c_ν and reference code $c_{r,\nu}$. A detailed derivation of (12) and (14) can be found in [7]. w_μ denotes the resulting complex-valued, zero-mean, additive white Gaussian noise with variance

$$\begin{aligned} \sigma_w^2 &= E \{ |w - E\{w\}|^2 \} = 2 \cdot E \{ w_I^2 \} = 2 \cdot E \{ w_Q^2 \} \\ &= L \cdot 2N_0 \cdot \frac{1}{T_s} \cdot F = \frac{L^2}{T_c} \cdot 2N_0 \cdot F. \end{aligned} \quad (14)$$

Due to cost constraints, e.g. the mobile phone crystal can be quite inaccurate. The oscillator of a mobile phone platform is then realigned with frequency correction signals from the cellular network, but for TDMA systems like GSM only at discrete points of time, while the oscillator drifts away in between. Compensating the frequency

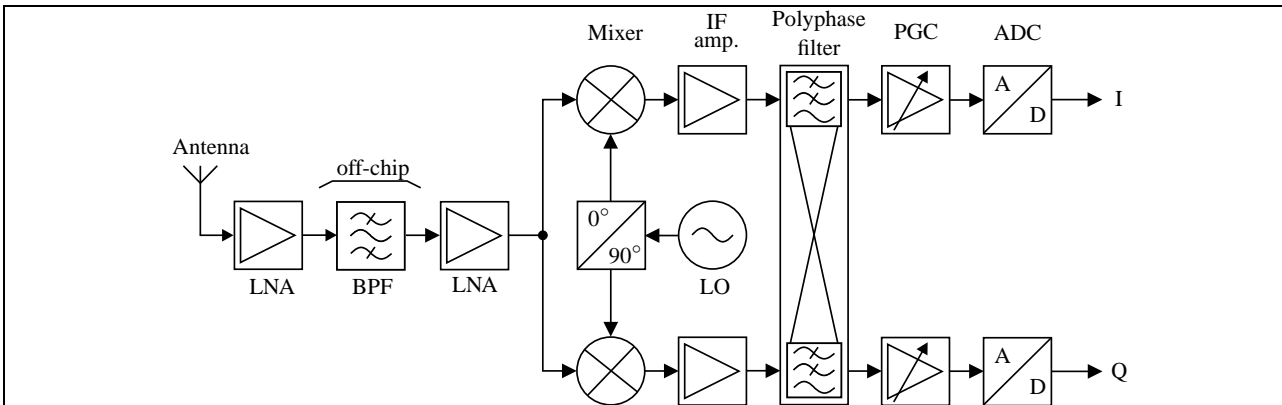


Fig. 1. Proposed low-IF front-end architecture for a combined Galileo/GPS receiver.

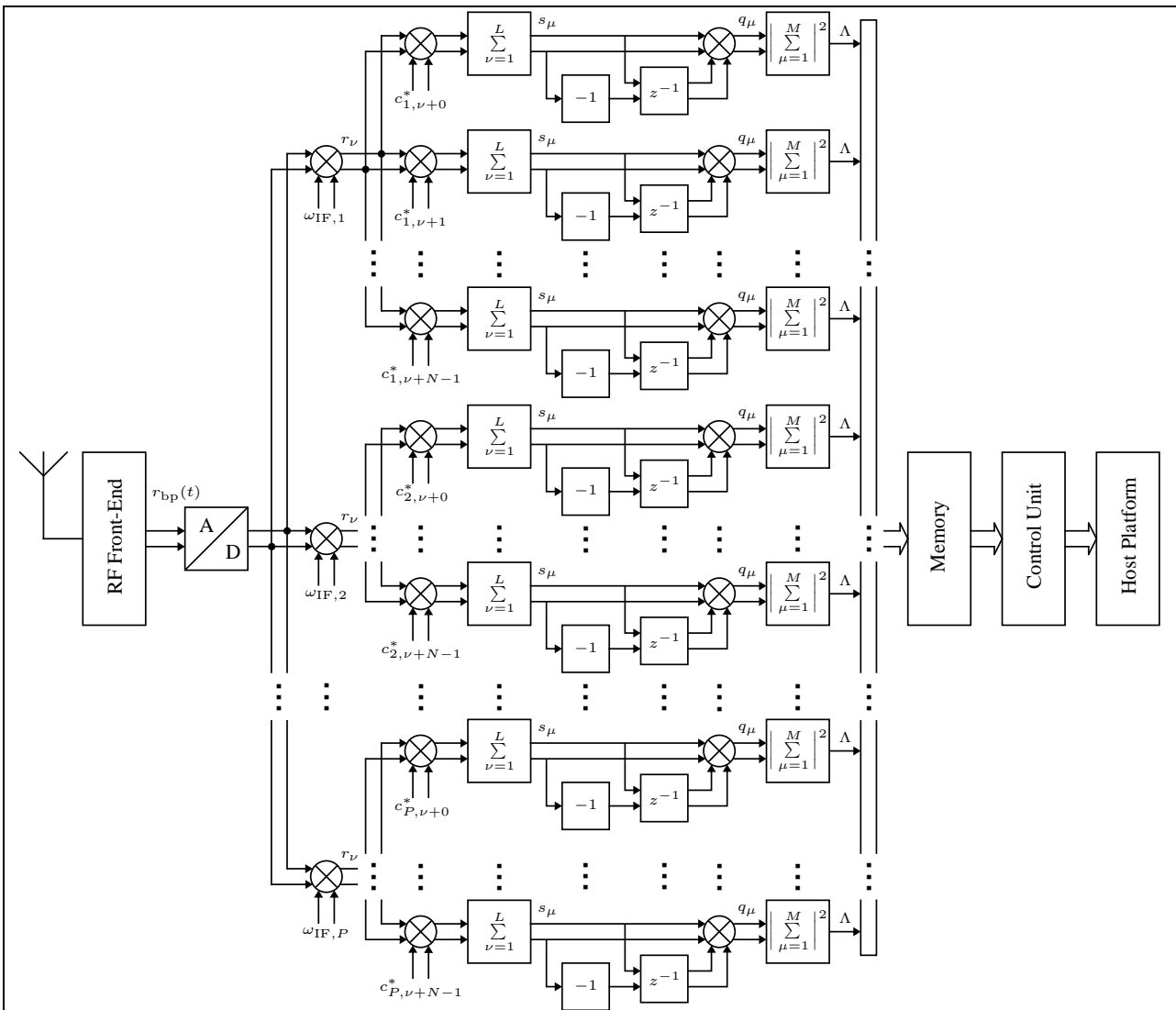


Fig. 3. Potential digital baseband architecture with differential correlation for single shot measurements.

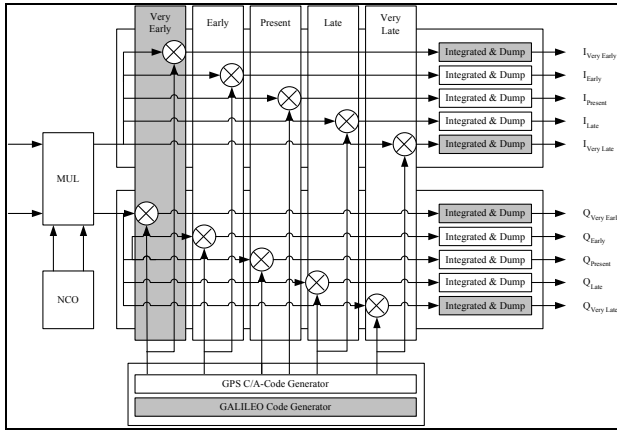


Fig. 4. Architecture of the combined GPS and Galileo correlator for the tracking process.

drift of the oscillator between the correction points can require a significant amount of additional signal processing [8]. Especially for long integration times (as required for moderate indoor conditions) the frequency drift during integration can become an important issue. Finding the best trade-off between oscillator cost and cost required for more sophisticated signal processing is an important target.

New signal processing challenges arise with the transition from GPS to combined GPS/Galileo, e.g. due to the BOC modulation scheme or longer PRN sequences. Therefore, a flexible architecture that enables reuse of communication and signal processing components throughout the different navigation standards is a possible solution for a multi-standard receiver. The received signal can either be correlated with a GPS or a Galileo code. The key issue in this architecture is the clock generation unit. Besides generating an appropriate chipping clock for the respective standard, it has to detect epoch boundaries, and generate synchronization signals (e.g. for switching between navigation standards).

The same principle can be applied to the correlation processor for tracking mode, presented in Fig. 4. Even though Galileo BOC signals require additional correlators (very-early and very-late replica codes besides the early, prompt, and late correlators for GPS C/A), the basic architecture remains the same. It is therefore possible, to form a combined correlation processor architecture, where the early-prompt-late correlator structure is used for GPS and Galileo, while the additional correlators required for Galileo are activated on demand. This allows to switch between GPS and Galileo signals during runtime.

5. Differential Correlation

For differential correlation, the current predetection sample after coherent integration is multiplied with the complex conjugated of the previous predetection sample after coherent integration [7]. This product is then further accu-

mulated

$$\tilde{\Lambda}_{\text{Diff}} = \sum_{\mu=1}^M s_{\mu} \cdot s_{\mu-1}^* \quad (15)$$

s_{μ} was defined previously in (12). Since the result is still complex-valued, the detector might take the squared envelope at the end of the accumulation process

$$\Lambda_{\text{Diff}} = \left| \sum_{\mu=1}^M s_{\mu} \cdot s_{\mu-1}^* \right|^2 \quad (16)$$

Differentially coherent integration as shown in (16) is an alternative method to conventional noncoherent integration

$$\Lambda_{\text{Std}} = \sum_{\mu=0}^M |s_{\mu}|^2 \quad (17)$$

Differential correlation allows to synchronize the spreading code phase with lower SNR degradation than conventional noncoherent integration [7]. Signal plus noise differentially correlated leads to

$$\begin{aligned} & s_{\mu} \cdot s_{\mu-1}^* \\ &= 2C \cdot d_{\mu} \cdot d_{\mu-1} \cdot R_{rc}^2(\tau) \cdot \text{si}(\pi \Delta \bar{f}_{\mu} \cdot T_c) \\ & \quad \cdot \text{si}(\pi \Delta \bar{f}_{\mu-1} \cdot T_c) \cdot e^{j \cdot [\pi(\Delta \bar{f}_{\mu} - \Delta \bar{f}_{\mu-1}) \cdot T_c + \varphi_{\mu} - \varphi_{\mu-1}]} \\ & \quad + \sqrt{2C} \cdot d_{\mu} \cdot R_{rc}(\tau) \cdot \text{si}(\pi \Delta \bar{f}_{\mu} \cdot T_c) \\ & \quad \cdot e^{j \cdot (\pi \Delta \bar{f}_{\mu} \cdot T_c + \varphi_{\mu})} \cdot w_{\mu-1}^* \\ & \quad + \sqrt{2C} \cdot d_{\mu-1} \cdot R_{rc}(\tau) \cdot \text{si}(\pi \Delta \bar{f}_{\mu-1} \cdot T_c) \\ & \quad \cdot e^{-j \cdot (\pi \Delta \bar{f}_{\mu-1} \cdot T_c + \varphi_{\mu-1})} \cdot w_{\mu} \\ & \quad + w_{\mu} \cdot w_{\mu-1}^* \quad , \end{aligned} \quad (18)$$

where all variables were defined in the previous chapter. The first summand represents the deterministic signal component. The second and the third summand are zero-mean complex Gaussian noise. The fourth summand is the product of two zero-mean complex Gaussian distributions, which results in a normal product distribution. The accumulation of (18) over M periods yields

$$\begin{aligned} \tilde{\Lambda}_{\text{Diff}} &= 2C \cdot R_{rc}^2(\tau) \cdot \sum_{\mu=1}^M \left[d_{\mu} \cdot d_{\mu-1} \cdot \text{si}(\pi \Delta \bar{f}_{\mu} \cdot T_c) \right. \\ & \quad \left. \cdot \text{si}(\pi \Delta \bar{f}_{\mu-1} \cdot T_c) \cdot e^{j \cdot [\pi(\Delta \bar{f}_{\mu} - \Delta \bar{f}_{\mu-1}) \cdot T_c + \varphi_{\mu} - \varphi_{\mu-1}]} \right] \\ & \quad + \sum_{\mu=1}^M u_{\mu} \quad , \end{aligned} \quad (19)$$

where u_{μ} denotes the combined noise component, which is comprehensively derived in [7]. The term $\Delta \bar{f}_{\mu} - \Delta \bar{f}_{\mu-1}$ represents the change of frequency deviation $\Delta \bar{f}_{\mu}$ from one coherent integration interval to the next one. Such a change can be introduced from a reference oscillator drift or a varying Doppler frequency. For a stable frequency deviation (i.e. $\Delta \bar{f}_{\mu} = \Delta \bar{f}_{\mu-1} = \Delta \bar{f} = \text{const.}$), the differential correlation delivers signal components that are all in

phase to each other

$$\tilde{\Lambda}_{\text{Diff}} \Big|_{\Delta\bar{f}=\text{const.}} = 2C \cdot R_{rc}^2(\tau) \cdot \text{si}^2(\pi\Delta\bar{f} \cdot T_c) \cdot e^{j \cdot 2\pi\Delta\bar{f} \cdot T_c} \cdot \sum_{\mu=1}^M d_{\mu} \cdot d_{\mu-1} + \sum_{\mu=1}^M u_{\mu} , \quad (20)$$

since

$$\varphi_{\mu} - \varphi_{\mu-1} \Big|_{\Delta\bar{f}=\text{const.}} = 2\pi\Delta\bar{f} \cdot T_c = \text{const.} . \quad (21)$$

A detailed analysis of differential correlation is provided in [7]. All deterministic and stochastic signal components with their probability distributions and moments are derived algebraically. The achievable sensitivity is calculated and compared to conventional noncoherent integration for cases with constant frequency deviation, frequency drift, and strong interfering navigation signals.

6. Multipath Mitigation

By narrowing the chip spacing d [chips] of the early and late correlators in a noncoherent DLL, e.g. 0.1 chip correlator spacing, the maximum multipath error is reduced by a factor of e.g. 10 and multipath with relative delays of approx. 1 chip or greater is rejected entirely [3]. The noise error is proportional \sqrt{d} . The basic concept of the E1/E2 Tracking correlation technique is to find a tracking point on the autocorrelation function that is not distorted by multipath. Two correlators with a chip spacing of d [chips] are located on the early slope of the autocorrelation function. In case that the actual position of the two correlators E1, E2 and the shape of the autocorrelation function is known, the amplitudes at both correlator positions can be used to set up an error function for this correlation technique

$$D(\tau) = \eta - \frac{R_{E2}(\tau)}{R_{E1}(\tau)} . \quad (22)$$

For a given tracking point τ_0 , η can be expressed as

$$\eta = \frac{\tau_0 - d + T_c}{\tau_0 + T_c} , \quad (23)$$

with d [chips] being the correlator spacing between E1 and E2 and T_c the chip length of code.

The multipath performance was simulated with the IfEN Monte Carlo simulator. The model is based on the multi-ray model used in the SNSS simulation tool of IfEN. For the distinct dominant reflectors the corresponding rays were generated with a constant delay and variable phase, varying with a Doppler between 0 and 0.017 Hz relative to the direct line-of-sight, as specified in the Galileo multipath model. For the diffuse component, a multitude of rays was generated. In order to maintain the constant overall power in the diffuse component, each ray was assigned

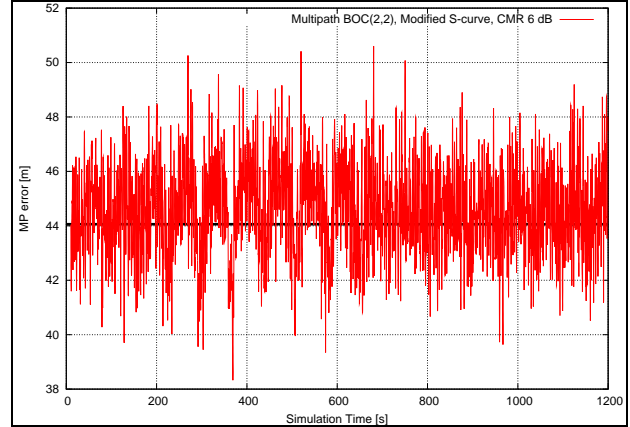


Fig. 5. Multipath error on L1 BOC(2,2) using the modified S-curve in 8 MHz bandwidth for the unfavorable multipath conditions with CMR = 6 dB.

an amplitude according to

$$a_i = \frac{1}{\sqrt{N}} 10^{-(CMR/20)} \quad (24)$$

for each part of the diffuse component, where N is the number of rays in each diffuse component and CMR the carrier to multipath ratio.

$N = 30$ was selected for the simulation. Increasing the number of rays in the diffuse components beyond 10 did not lead to a significant change in the multipath behavior. The Doppler for the diffuse component was random with a uniform distribution between 0 and 0.1 Hz. The delays were also random uniformly distributed. A time series for the duration of 1500 s was generated for each elevation angle (15° , 50° and 90°).

Fig. 5 shows a multipath simulation for the Galileo BOC(2,2) signal with 8 MHz bandwidth and CMR = 6 dB. The receiver model is a first order, non-coherent early-late DLL with 1 Hz bandwidth and a second order Costas PLL with 10 Hz bandwidth. The DLL is aided with the PLL (carrier aiding). For multipath mitigation, a narrow correlator with 0.1 chip spacing and the E1/E2 Tracking technique with $\eta = 0.35$ is simulated. The correlation functions generated by IfEN's SNSS simulation tool contain a bias that is caused by the filtering. This bias is not relevant for the positioning, since all signals are subject to it and thus the bias is global and is inseparable from the receiver clock. The bias caused by filtering for Fig. 5 is 44.06 m. When analyzing the multipath error it is of interest what error is generated by the multipath. This error, however, is not identical on all lines-of-sight. The simulations show, that the mean value for the modified S-curve is about 54 cm and a standard deviation (1σ) of 1.6 m.

7. Acquisition Performance

The acquisition performance limit of the standard noncoherent acquisition scheme described by [4]

$$\Lambda = \sum_{\mu=1}^N (I_{\mu}^2 + Q_{\mu}^2) = I_1^2 + Q_1^2 + I_2^2 + Q_2^2 + \dots \quad (25)$$

is shown in Fig. 6 and 7. The results are compared to a variant of differential correlation, described by

$$\begin{aligned} \Lambda &= \sum_{\mu=1}^N (I_{2\mu} \cdot I_{2\mu-1} + Q_{2\mu} \cdot Q_{2\mu-1}) \\ &= I_2 \cdot I_1 + Q_2 \cdot Q_1 + I_4 \cdot I_3 + Q_4 \cdot Q_3 + \dots \end{aligned} \quad (26)$$

Fig. 8 compares the performance of both when only thermal noise interference is present. A theoretical derivation of the probability density functions for hypothesis H_0 (cross-correlation) and H_1 (correlation peak) of this model is presented in [1]. The sensitivity of the algorithms is estimated by calculating the minimum required C/N_0 necessary to detect the signal for a probability of detection $P_d = 0.9$ and a probability of false alarm $P_f = 0.005$. N denotes the noncoherent or differential integration number, respectively and L the coherent integration number. Degradation due to Doppler frequency shift and implementation nonidealities are neglected for these simulations. For an appropriate comparison of the algorithms according to (26) and (25) in Fig. 8 and Fig. 9, the noncoherent integration number N for the variant of differential correlation is half the noncoherent integration number N for the standard algorithm. A substantial improvement of up to 2 dB is observed with respect to the standard noncoherent algorithms when only white Gaussian noise is present. The predictions were confirmed by implementing the algorithms in the Institute of Geodesy and Navigation PC-based Experimental Software Receiver (ipexSR) [6].

For indoor positioning scenarios it is important to study the effect of the presence of a strong navigation signal on the desired weak signal during the acquisition. The respective simulations in Fig. 6 and Fig. 7 assume an interfering signal of 50 dBHz that results in a 29 dBHz interference signal if the cross-correlation value between the strong and weak signal is assumed to be -21 dB. Fig. 9 compares the variant of differential correlation algorithm versus the standard noncoherent algorithm when a strong interfering GPS signal is present.

8. Navigation Software

The presence of more than 50 satellites, GPS and Galileo, significantly enhances the navigation accuracy particularly in difficult surroundings like urban areas. The navigation solution has then to be calculated through a combination of Galileo and GPS C/A signals. Depending on the availability of satellites, the navigation software can determine the receiver position by different modes, as presented in 2. When more than four satellites and pseudo-range measurements are available, the receiver state deter-

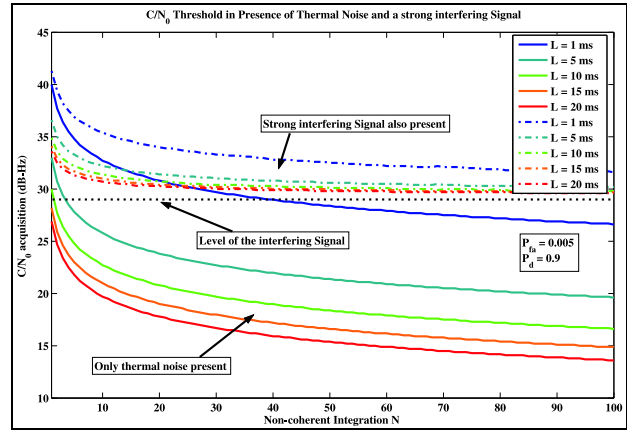


Fig. 6. Minimum required C/N_0 for acquisition using the standard noncoherent algorithm in presence of thermal noise and a strong signal of 50 dBHz with a cross-correlation value of -21 dB.

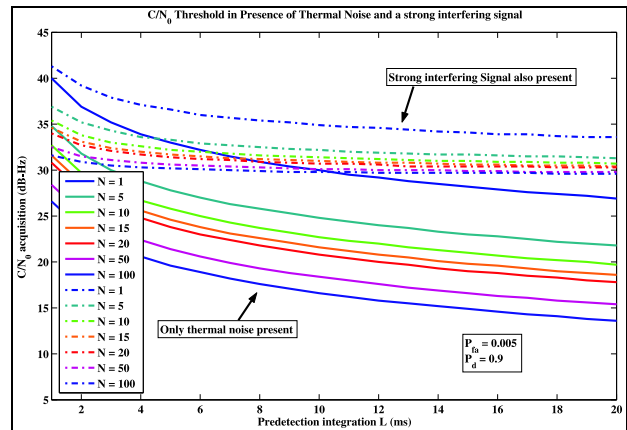


Fig. 7. Minimum required C/N_0 for acquisition using the standard noncoherent algorithm in presence of thermal noise and a strong signal of 50 dBHz with a cross-correlation value of -21 dB.

mination (position, velocity, clock bias, and clock drift) is done classically using Kalman filtering.

To speed up the computation by reducing the search space and to aid the reacquisition of lost satellites, the Doppler shift for the next epoch is predicted. Another advantage of the new navigation software is the computation of the receiver position on the basis of code phase measurements. Only using the code phase introduces an ambiguity that can be resolved by using an approximate user position. The single shot positioning mode is developed for applications like mobile phones where minimum power consumption is an important requirement. It is planned to aid the positioning algorithm by additional information, such as the mobile phone cell ID. Additionally, the navigation software offers a continuous positioning mode, developed for automotive applications.

Table 2. Position determination in case of degraded satellite availability.

| Satellites in View | Position Determination |
|--------------------|--|
| ≥ 4 | 3D-Positioning with Receiver Clock Error Estimation |
| 3 | 3D-Positioning without Clock Error Estimation or 2D-Positioning with Receiver Clock Error Estimation |
| 2 | 2D-Positioning without Receiver Clock Estimation |
| 1 | 1D-Positioning Prediction of User Position Based on Previous Trajectory |

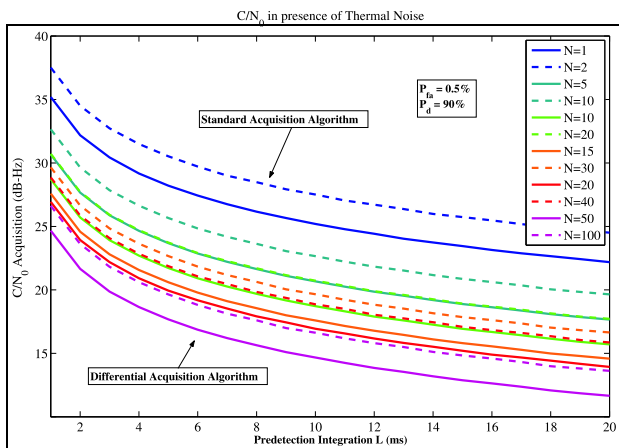


Fig. 8. Minimum required C/N_0 for acquisition in presence of thermal noise. The solid lines correspond to the standard noncoherent algorithm while the dashed lines refer to the variant of differential acquisition algorithm.

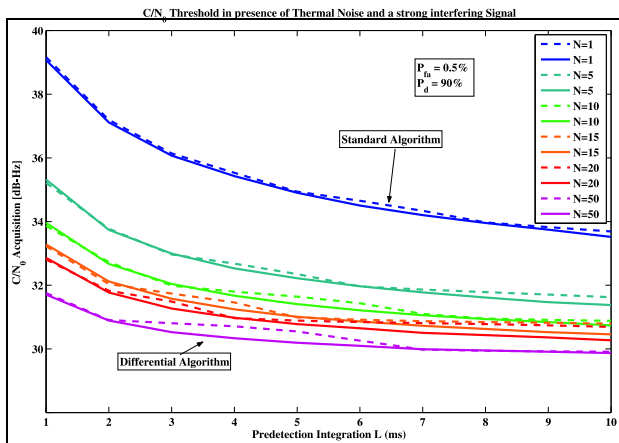


Fig. 9. Comparison of the performance of the standard noncoherent algorithm versus the variant of differential correlation algorithm in presence of a strong interfering signal. The performance of the standard noncoherent algorithm is shown in dashed line, while that of the variant of differential correlation algorithm has solid lines.

9. Conclusion

The paper has outlined a combined Galileo/GPS receiver concept to be developed during the first phase of the HIGAPS project. It is specially tailored for location based services, E-911, and consumer market applications. A customized receiver architecture was presented in order to meet the extraordinary important requirements of low cost, low energy consumption, and enhanced sensitivity.

The low-IF topology of the RF front-end circumvents the well-known problems of zero-IF topologies. The highly parallel digital baseband architecture utilizes the benefits of a low-power, high integration CMOS process. It enables single shot measurements with short time to fix, high sensitivity, low power consumption, and low implementation complexity. Differential correlation provides sensitivity gain compared to conventional noncoherent integration. An adequate navigation processor has to support single shot measurements and jointly utilize Galileo and GPS.

Acknowledgement

The investigations and developments of this work are supported within the scope of the research project HIGAPS, which is jointly sponsored by the Bavarian Ministry of Economic Affairs, Infrastructure, Transport and Technology, as well as the German Aerospace Center (DLR).

References

- [1] J.A. Ávila-Rodríguez, B. Eissfeller, and T. Pany, "A Theoretical Analysis of Acquisition Algorithms for Indoor Positioning", *ESA ESTEC NAVITEC 2004*, Dec. 2004.
- [2] J. Crols and M.S.J. Steyaert, "Low-IF Topologies for High-Performance Analog Front Ends of Fully Integrated Receivers", *IEEE Transactions on Circuits and Systems-II*, vol. 45. no. 3, pp. 269-282, March 1998.
- [3] A.J. Van Dierendonck, P. Fenton, and T. Ford, "Theory and Performance of Narrow Correlator Spacing in a GPS Receiver", *Navigation*, vol. 39, no. 3, pp. 265-283, 1992.
- [4] A.J. Van Dierendonck, "GPS Receivers", *Global Positioning System: Theory and Applications*, vol. 1, eds. B.W. Parkinson and J.J. Spilker, American Institute of Aeronautics and Astronautics, 1996.
- [5] G.W. Hein, et al., "Performance of Galileo L1 Signal Candidates", *Proc. European Navigation Conference GNSS 2004*, May 2004.
- [6] T. Pany, B. Eissfeller, and G.W. Hein, "ipexSR: the First PC Based Software GNSS Receiver Completely Developed in Europe", *Proc. European Navigation Conference GNSS 2004*, May 2004.
- [7] A. Schmid and A. Neubauer, "Performance Evaluation of Differential Correlation for Single Shot Measurement Positioning", *Proc. Institute of Navigation GNSS 2004*, Sept. 2004.
- [8] L. Vittorini and B. Robinson, "Frequency Standards: Key Enabler to Optimizing Indoor GPS Performance", *Proc. Institute of Navigation GPS/GNSS 2003*, pp. 660-671, Sept. 2003.